JACS
JOURNAL OF THE AMERICAN CHEMICAL SOCIETY
Article
pubs.acs.org/JACS

Mapping the Energy Distribution of SERRS Hot Spots from Anti-Stokes to Stokes Intensity Ratios

Diego P. dos Santos,[†,‡] Marcia L. A. Temperini,[†] and Alexandre G. Brolo*[,‡]

[†]Instituto de Química, Universidade de São Paulo, CP 26.077, CEP 05513-970, São Paulo, SP, Brazil
[‡]Department of Chemistry, University of Victoria, P.O. Box 3065, Victoria, BC, Canada, V8W 3 V6

Supporting Information

ABSTRACT: The anomalies in the anti-Stokes to Stokes intensity ratios in single-molecule surface-enhanced resonance Raman scattering were investigated. Brilliant green and crystal violet dyes were the molecular probes, and the experiments were carried out on an electrochemically activated Ag surface. The results allowed new insights into the origin of these anomalies and led to a new method to confirm the single-molecule regime in surface-enhanced Raman scattering. Moreover, a methodology to estimate the distribution of resonance energies that contributed to the imbalance in the anti-Stokes to Stokes intensity ratios at the electromagnetic hot spots was proposed. This method allowed the local plasmonic resonance energies on the metallic surface to be spatially mapped.

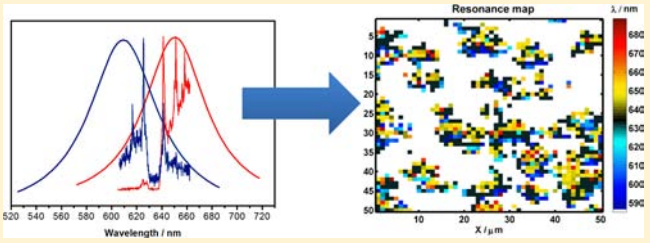

1. INTRODUCTION

The fluctuations in surface-enhanced Raman scattering (SERS) intensities for experiments in diluted solutions are the result of a small number of molecules probing special surface regions, known as the "SERS hot spots".[1] In the absence of photothermal and photochemical effects, the origin of the intensity fluctuations is simply explained by considering that, by chance, a molecule adsorbs on a highly efficient hot spot long enough to generate a Raman signal that overcomes the detection limit of the measuring system. Experiments with two analytes are a direct proof that the regime of SERS intensity fluctuations is related to the single-molecule capability of the technique.[2]

The single-molecule limit is achieved at the hot spots by contributions from a set of resonance factors that might include the localized surface plasmons resonance (LSPR), the charge-transfer resonance involving the metal-molecule complex system, and the resonance Raman effect of the adsorbate molecule.[3] It is accepted that the contributions from LSPRs to the overall intensity are the most important in the majority of cases. In that sense, the *distribution of SERS intensities* in the regime of strong fluctuations is then directly related to the *distribution of local electric field strengths* at the hot spots. Local enhancement factors as low as $\sim 10^8$ are believed to be sufficient for single-molecule detection.[1b,2a,4] The effect of the described resonances is not restricted to improve the detection limit of the technique. The resonances also affect the dynamics of the fluctuations, as observed by the changes in relative intensities and peak shifts during the spectral fluctuations.[1d,5]

Another very interesting effect observed in the regime of strong SERS intensity fluctuations is the unusually high anti-Stokes intensities (relative to the Stokes scattering) for a few events. Reported initially by Kneipp et al.,[6] this phenomenon was first interpreted as resulting from a stimulated pumping process that increased the population of excited vibrational states. Although the vibrational pumping mechanism might play a role at cryogenic temperatures,[7] other authors demonstrated that the high anti-Stokes to Stokes ratio could be explained by a resonance model instead.[8] The argument is based on the fact that the magnitude of the anti-Stokes to Stokes ratios fluctuates in time, and enhanced Stokes events, relative to the anti-Stokes intensities, are observed as well (those cannot be explained using the optical pumping mechanism).

According to the resonance model, a molecule that adsorbs on a hot spot with resonance contributions that coincides with the Stokes scattering would show preferential enhancement of the Stokes side. On the other hand, anti-Stokes scattering would be enhanced, relative to the Stokes, when the molecule visits a hot spot with resonance energy that is shifted into the anti-Stokes side. This preferential enhancement of either the Stokes or anti-Stokes intensities due to resonances is well-known in the resonance Raman literature.[9] Therefore, in the regime of strong fluctuations of SERS intensities, the *distribution of anti-Stokes to Stokes ratios* should then be directly correlated to the *distribution of resonance energies at the hot spots*.

We have recently reported that, in electrochemical conditions, the distribution of anti-Stokes to Stokes ratios can be modulated by the applied potential.[10] The observations were in agreement with a resonance factor set by the applied potential, which is a well-established feature in electrochemical SERS measurements.[3c,11] In the present work, we suggest a methodology to estimate the distribution of plasmonic hot spot energies that contribute to the imbalance of the anti-Stokes to

Received: June 8, 2012
Published: July 17, 2012

   dx.doi.org/10.1021/ja305580t | J. Am. Chem. Soc. 2012, 134, 13492−13500

Stokes intensity ratios. The distribution was estimated by monitoring the anti-Stokes to Stokes ratios under the conditions of strong intensity fluctuations. Although the energy of the plasmonic hot spots can, in principle, be obtained by near-field optical methods,[12] the procedure developed here provides a simpler alternative and allows a better understanding of the nature of the anomalous intensity fluctuations under dynamical conditions. Our results also show that the fluctuations in anti-Stokes to Stokes ratios can also be used as an additional tool to confirm single-molecule behavior in SERS measurements.

2. EXPERIMENTAL SECTION

2.1. Materials. Crystal violet (CV) and brilliant green (BG), both from Aldrich, were used as received without any further purification. Stock solutions were prepared in ethanol (Synth), and dilutions were made in deionized water (USF Elga, Maxima, model Scientific MK3, 18.2 MΩ·cm).

2.2. Electrochemical Measurements. The electrochemical measurements were done by using an EG&G potentiostat model PAR-273. The SERS substrate used was an Ag electrode activated by oxidation and reduction cycles (ORCs). The working electrode was a polycrystalline Ag (99.99%, Aldrich, diameter = 0.13 cm) rod inserted in a Teflon sleeve, which was mechanically polished before the ORCs with 600 mesh and subsequently with 1200 and 2000 mesh sandpaper and thoroughly rinsed with deionized water. The reference and auxiliary electrodes were Ag|AgCl|$KCl_{(sat)}$ and a platinum wire, respectively. The details of the ORC procedure are well described elsewhere.[13] Briefly, the working electrode was submitted to 3 cycles of oxidation and reduction in the range of potentials between −0.3 and +0.3 V at a scan rate of 50 $mV{\cdot}s^{-1}$. The electrolyte solution was aqueous KBr 0.1 $mol{\cdot}L^{-1}$. Bromide ion was used instead of chloride (electrochemical SERS activation is generally done in KCl) to prevent the appearance of Raman signals due to the anion adsorbed on the Ag surface, which would interfere with the lowest frequency band of each of the dyes used. The Ag^0−Br stretching is around 160 cm^{-1} and, therefore, does not interfere with the low-frequency band of the investigated dyes at ∼200 cm^{-1}.[14]

The roughening process was done in the absence of the dyes (CV and BG) that were added to the solution after the activation to the desired concentration.

2.3. SERRS Measurements. Surface-enhanced resonance Raman scattering (SERRS) mapping (both dyes show electronic transitions close to the excitation energy; therefore, the acronym SERRS will be used throughout the text) from solutions containing BG and CV, both at a concentration of 10 nM each (bianalyte experiment), was obtained using a Renishaw in-Via microscope, equipped with a 63× water immersion objective (NA = 0.9). The excitation wavelength was 632.8 nm from a He−Ne source (Renishaw RL6333), and the mapped area was 50 × 50 μm^2, with 1 μm step (total of 2500 spectra per map). The laser power at the sample was estimated to be on the order of 2 μW, the illuminated area was about 1 μm^2, and the integration time was of 1 s. The low laser power was used to prevent photodecomposition of the dyes and the local heating of the Ag surface. The spectra were acquired using a 600 L/mm grating, which covers a spectral range of around 1400 cm^{-1}, allowing the simultaneous measurement of the anti-Stokes and Stokes signals.

2.3. Data Analysis. The separation and identification of the CV and BG spectra in the collected data were done by using the modified principal component analysis (MPCA) approach, after background removal with the program COBRA.[15] The MPCA method is based on a second step performed on the principal component analysis (PCA) to extract the independent features of the obtained components, as described by Etchegoin et al.[2a] The method allows a direct correlation between each principal component and the SERRS spectrum of each dye in the solution. All PCA and MPCA analyses were done with the R 2.7.0 software.[16]

3. RESULTS AND DISCUSSION

3.1. The Statistical Methodology. The premise of our model is that the fluctuations in SERRS signals, which only appear in the regime of low analyte concentrations, are directly related to molecules visiting hot spots on the electrode surface. There are basically two experimental approaches to monitor those fluctuations: One is to fix the laser at a particular surface spot and obtain thousands of consecutive spectra against time, and the second is to SERRS-map a predetermined area. In that case, some spots at the surface will present a signal, but most of the areas will yield no spectrum.[17] Although we have previously obtained and analyzed the time evolution of the Stokes and anti-Stokes intensities from a fixed spot,[10] the results presented in this work are for spectra obtained using the SERRS mapping approach. The advantage of using mapping is that the laser briefly illuminates each spot (only 1 s for the experiments reported here), decreasing the issues of photodecomposition that might occur when the same spot is probed for a long time. Furthermore, from the mapping measurements, it is possible to sample a larger number of hot spots, which gives more confidence to the statistical analysis, assuming that the hot spot distribution is completely random due to the nature of the surface roughness. The mapped area in each experiment (50 × 50 μm) yielded 2500 spectra, which were analyzed using the MPCA method. The first and the second principal components obtained after the MPCA analysis of the Stokes region during one mapping experiment (2500 spectra) are presented in Figure 1a. The results in Figure 1 are from an aqueous solution containing a mixture of 10 nM of each CV and BG. The two MPCA components in Figure 1a, MPCA1 and MPCA2, can be directly compared to the SERRS of each dye at 1 μM, presented as an inset in Figure 1a, obtained in separate experiments. The spectra of the dyes at 1 μM did not present the strong SERRS fluctuations observed from the 20 nM solutions. This is because at concentrations of the dyes in the μM range (and higher), most of the surface area is covered by the dye molecules, including all the hot spots, leading to an average SERRS signal that does not significantly change with time. We will then call the conditions of "high" concentrations of the dyes (1 μM) "average SERRS", in contrast to the term "single-molecule" condition that will be used in the text for the SERRS results obtained in the low-concentration regime (20 nM concentration of the dyes). It is clear from Figure 1a that the SERRS band at 198 cm^{-1} can be uniquely assigned to CV, and the band at 219 cm^{-1} is due to BG.

The MPCA components obtained from the analysis of 2500 spectra (Figure 1a) are very similar to the average SERRS spectra from BG and CV (presented as an inset in Figure 1a). The result from Figure 1a leads then to the identification and separation of the spectra of each dye in the data set by the relative contribution of each of the MPCA components. In other words, each of the 2500 spectra is decomposed in their principal components and analyzed to check for the presence of MPCA1 and MPCA2. This permits the generation of a histogram indicating the contribution of each of these dyes to each spectrum. Figure 1b shows the counting (histogram) for one of the data sets. The histogram indicates the number of spectra where only vibrational features uniquely assigned to either BG or CV can be identified after the MPCA analysis. It also includes the number of events containing a mixture of both dyes (which are as important as the BG and CV only events, as it will be explained later) and all the events that contain just

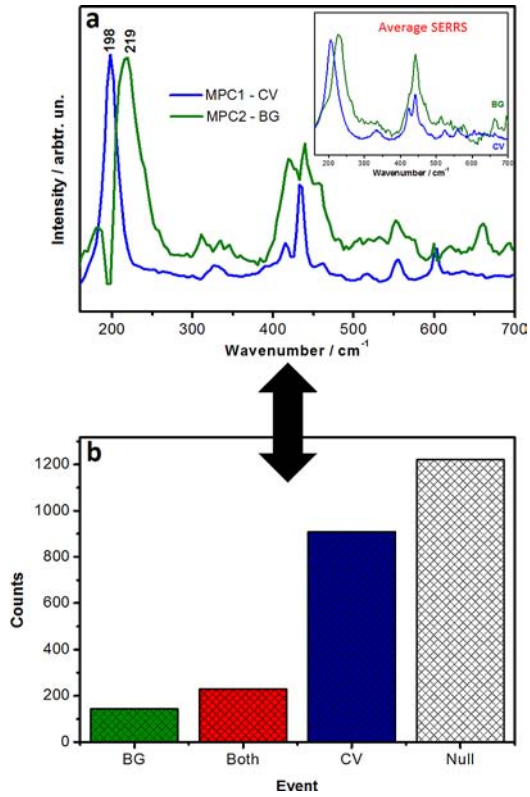

Figure 1. (a) Calculated MPCA components obtained from a SERRS map of the silver electrode in contact with a solution containing 20 nM of both dyes (CV and BG). The inset shows the "average SERRS" (from 1 μM solutions) of BG and CV. (b) Histogram calculated from the analysis of the SERRS map. The counts indicate BG only, CV only, both, and null events observed for the 2500 spectra obtained after the MPCA treatment.

noise (spectra with no features assignable to either dye molecule, indicated as null events in the histogram).

In a model that considers a small number of adsorbates interacting with the several hot spots at the surface, the presence of spectra containing vibrational features from just one of the dyes (either BG or CV), as shown in Figure 1b, is consistent to single-molecule behavior, since it would be statistically unlike that only one type of molecule from a mixture would populate a large fraction of the surface in a given time. Some differences in the adsorption properties of each dye are expected (because they are two chemically distinct species), which is consistent with the occurrence of a larger number of single CV spectra, in comparison to BG, in Figure 1b. This difference in adsorption properties can be tuned by the applied potential (Figure 1 was obtained at open circuit potential), as reported before.[13a]

3.2. Analysis of Anti-Stokes to Stokes Ratios Distribution under Average SERRS Conditions. After the extraction and characterization of the contribution from each dye in every event in a data set, the anti-Stokes to Stokes intensity ratios (ρ) were calculated using the 198 cm^{-1} band for CV and the 219 cm^{-1} band for BG. Figure 2a shows a histogram for the values of ρ obtained in the average SERRS conditions for BG (green) and CV (blue). In this case, the SERRS mapping presents spatial variation in intensities (but no significant time-dependent intensity fluctuations), as expected from a roughened electrode. The values of ρ follows a normal distribution centered at $<\rho_{BG}> = 0.15 \pm 0.05$ for BG and $<\rho_{CV}> = 0.22 \pm 0.08$ for CV. The average values, 0.15 and 0.22, are smaller than the expected from a Boltzmann distribution at 298 K (the approximate temperature the experiments were carried out). The expected thermal ρ value was 0.28. The smaller ρ values relative to the Boltzmann case, obtained from the average SERRS experiments, are not due to instrumentation artifacts, since we have verified that ρ for pure carbon tetrachloride measured in the same conditions was very close to the expected from the simple thermal equilibrium assumption.[10] Therefore, the experimental results from Figure 2a show that, on average, the Stokes side of the SERRS spectrum is preferentially enhanced over the anti-Stokes (relative to expected from the thermal, Boltzmann, equilibrium) for the dyes investigated in this work.

Deviations for the ρ values from the expected thermal behavior are well-known in the resonance Raman literature.[9] Under resonance Raman conditions, the electronic envelop around the excitation wavelength dictates in which Raman branch (Stokes or anti-Stokes) a vibrational transition is preferentially enhanced, leading to deviations from the expected by a simple Boltzmann distribution. In another words, the assumption that both Stokes and anti-Stokes transitions have the same Raman cross-section breaks down under resonance conditions.

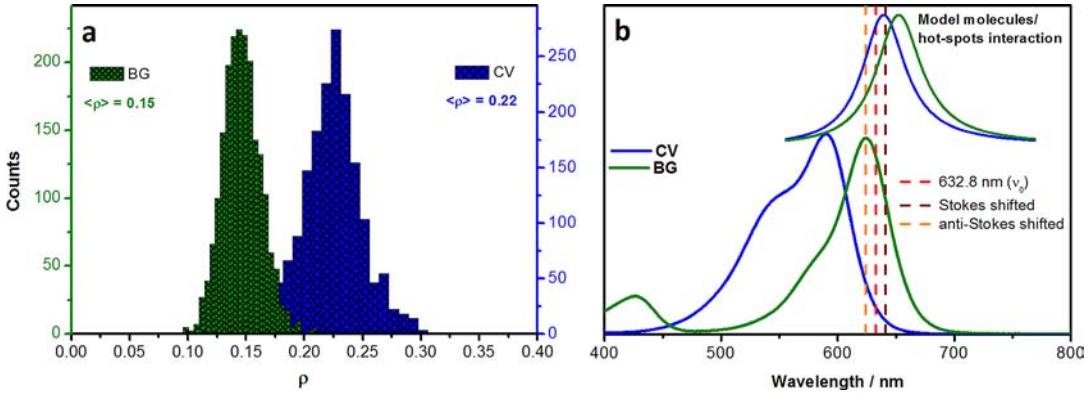

Figure 2. (a) Histograms for the anti-Stokes to Stokes intensity ratios (ρ values) in average SERRS conditions for BG (green) and CV (blue). The mean values for each distribution are shown in the figure. (b) UV–vis spectra for CV and BG in aqueous solution and a model showing the average resonance at the hot spots. The dashed lines correspond to the position of the laser excitation and the Stokes and anti-Stokes energies.

dx.doi.org/10.1021/ja305580t | J. Am. Chem. Soc. 2012, 134, 13492–13500

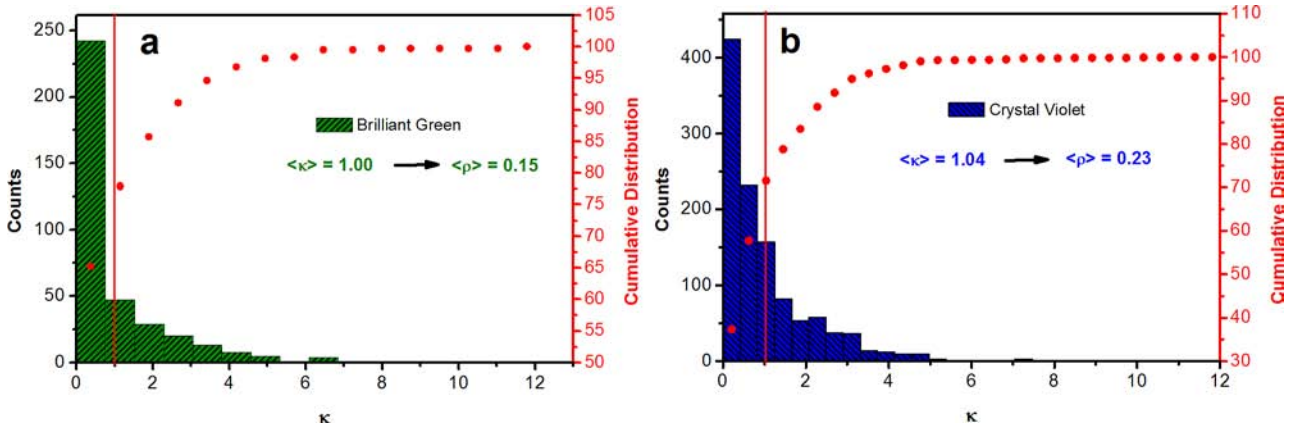

Figure 3. Histograms of the κ values (discussed in the text) for the "single-molecule" bianalyte experiment. Two histograms: (a) BG and (b) CV are presented. The cumulative distributions are also shown to illustrate the percentage of events with values smaller and larger than the average ($\kappa = 1$).

The electronic absorption (UV−vis) spectra for BG and CV in aqueous solutions are shown in Figure 2b. The dashed lines show the wavelengths of the laser and the Stokes- and anti-Stokes-shifted photons. It can be seen in Figure 2b that the electronic profiles of both dyes in solution overlap better with the anti-Stokes energy than with the Stokes (when excited with 632.8 nm). Therefore, a larger cross section for the anti-Stokes transition relative to the thermal equilibrium and a ρ-value larger than 0.28 (thermal value) were expected by just considering a resonance Raman model for the nonadsorbed molecules. (We are considering the Raman bands at ∼200 cm^{-1}, which are assigned to a mixture of stretching and bending between the central carbon atom of the molecule and the phenyl-substituted rings. These vibrations are part of the chromophore, since the main electronic transition in the UV−vis spectra of the dyes is assigned to a charge transfer from the phenyl-substituted rings to the central positively charged carbon atom.)[18] However, the ρ values obtained from the average SERRS measurements (Figure 2a) indicated preferential enhancement of the Stokes transitions instead. This suggests that the resonance condition for the adsorbed molecule is red-shifted relative to the electronic transitions in solution. The new resonance conditions for the adsorbed molecules are represented by the model curves presented in Figure 2b. The positions and the shapes of the model curves were calculated based on the experimental average ρ values obtained by SERRS (Figure 1a). The details of this resonance model are presented in the Supporting Information (SI) material.

The results from Figure 2 already provide some important fundamental insights into the SERRS mechanism. First of all, it shows that the resonance experienced by the molecule at the hot spot is not dictated solely by the electronic properties of the molecular probe. In fact, the anti-Stokes to Stokes intensity ratios for CV under resonance Raman conditions reported in the literature[19] show strong deviations relative to Figure 2a. This further confirms that the ρ values from Figure 2 cannot be attributed to a pure resonance Raman effect. Second, the fact that different molecules present different ρ value distributions (Figure 2a) indicate that the plasmonic excitation alone does not define the resonance experienced by the molecule at the hot spot either (if that was the case, both molecules should have presented the same ρ values distribution). Hence, the results in Figure 2 strongly suggest that the resonance environment experienced by the adsorbed molecule is a condition generated from a combination of contributions, probably from chemical, electronic, and plasmonic effects. An "unified SERRS" theory that takes into account all these effects has been suggested by Lombardi et al.[3a,b] A discussion of that model in the context of preferential anti-Stokes or Stokes resonances is presented in the SI. The key idea is that the different effects (chemical, electronic and plasmonic) contribute to a total SERRS intensity profile (or to a total enhancement factor profile) that can be modeled by a combination of Lorentzian functions. (The enhancement factor is defined as the ratio between the SERRS intensity of a single-molecule and its normal Raman intensity.)

Near-field optical microscopy is a technique capable of estimating the average hot spot resonance from SERS substrates. However, that technique probes the plasmonic contribution to the resonance. Figure 2 suggests that the resonance environment (resonance environment defined as plasmonic + molecular resonances) can be significantly modified by the presence of the molecular probe. The method suggested here, shown in Figure 2, provides a direct way to obtain the average resonance experienced by a species on a SERS substrate that encompasses molecular effects.

3.3. Analysis of Anti-Stokes to Stokes Ratio Distributions under Single-Molecule SERRS Conditions. The results presented in Figure 2 were obtained using dye concentrations in the 1 μM regime (average SERRS condition). However, when the concentration of the dyes was decreased to 10 nM each, strong intensities fluctuations were observed, characterizing the "single-molecule regime". These strong fluctuations in intensities were accompanied by a wide variation in the ρ values observed for each event. In order to quantify the deviation in the ρ values relative to the average SERRS behavior a normalized quantity (κ), defined in eq 1, was calculated for each event.

$$\kappa = \frac{\rho_{sm}}{<\rho_{average}>} \quad (1)$$

In eq 1, the subscripts "sm" and "average" refer to "single-molecule" and "average" SERS conditions, respectively. The < > indicates the mean value of the ρ values normal distribution for the average SERRS conditions, which is presented in Figure 2a. According to this definition, events with $\kappa = 1$ present anti-Stokes to Stokes ratios equal to the average SERRS values. On

dx.doi.org/10.1021/ja305580t | J. Am. Chem. Soc. 2012, 134, 13492−13500

the other hand, $\kappa < 1$ and $\kappa > 1$ are for Stokes- and anti-Stokes-enhanced events, relative to the average, respectively.

Notice that the definition of κ values allowed the same vibrational bands, experimental conditions, including temperature, and geometry to be used in the normalization, thus, there is no requirement to introduce other corrections to eq 1.

Histograms of κ for each dye, following the MPCA analysis in the "single-molecule" condition, are presented in Figure 3. The average κ values, calculated from the histograms in Figure 3, were equal to 1.00 and 1.04 for BG and CV, respectively, i.e., $<\rho_{BG}>$ and $<\rho_{CV}>$ are equal to 0.15 and 0.23. These are roughly the same ρ values obtained from the average SERS distributions in Figure 2a. This clearly shows that the average SERS signals are originated from the linear combination of contributions from all individual hot spots illuminated during a SERRS measurement.

The distributions of κ show higher contribution of ratios with $\kappa < 1$ for both dyes (about 70% of events for both histograms; see cumulative distribution values in Figure 3), which translates into a larger number of Stokes-enhanced events. Figure 3 also shows the presence of events with high κ values (>1) as well, characterizing anti-Stokes-enhanced spectra for both dyes.

It is interesting to notice that the range of κ values in the histograms in Figure 3 is the same for both dyes. This might suggest that the normalization used to generate κ eliminates the specific molecular effects. In that case, the resulting molecular-independent κ distribution should reflect the underlying plasmonic contribution to the overall enhancement. This assumption can be further justified by considering that the local electromagnetic (EM) resonance varies widely in a rough substrate, because it depends on the local geometric parameters of the nanostructure, while the molecular resonances are invariant. This model is illustrated in the SI (Figure S2).

3.4. Using the Anti-Stokes to Stokes Ratio from Bianalyte Experiments to Confirm the Single-Molecule Characteristic of SERRS. In Section 3.3, it was suggested that specific plasmonic resonances contributing to the anti-Stokes to Stokes intensity ratios anomaly can be isolated from chemical effects. The energy of those resonances will be estimated in Section 3.5. However, before the description of the methodology to obtain those resonances, we will discuss an interesting fundamental consequence of the analysis of the anti-Stokes to Stokes intensity ratios fluctuations. A close analysis of the individual events during the fluctuations in the experiments with low concentration of the dyes (10 nM) leads to another avenue to verify the single-molecule characteristic of SERRS. Figure 4 presents three selected spectra for events where spectral signatures of both dyes were identified (~198 and ~219 cm^{-1} for CV and BG, respectively; see Figure 1a). The negative wavenumber values correspond to the anti-Stokes region.

The point of Figure 4 is to illustrate that the observed κ values were not always the same for BG and CV in a given event, when the spectral signature for both dyes was observed simultaneously. For instance, Figure 4a,b shows events where both dyes have approximately the same κ values. Figure 4a is a case where the Stokes side is more intense than expected by a Boltzmann distribution for both dyes. The anti-Stokes side is strongly enhanced, relative to the Stokes, in Figure 4b. Figure 4c, however, shows a situation where very different κ values are observed for each species. For BG, the Stokes signal (at 219 cm^{-1}) is stronger than the anti-Stokes. On the other hand, for CV the band at 198 cm^{-1} in Figure 4c shows a larger anti-

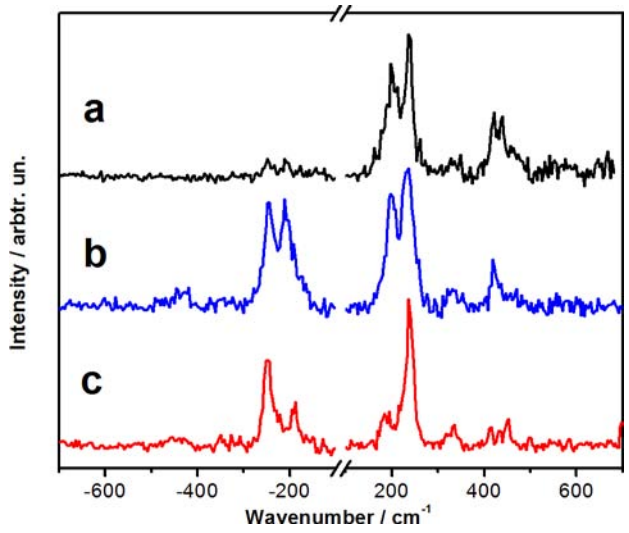

Figure 4. Selected spectra from a data set for a bianalyte experiment (BG and CV) in single-molecule conditions. The selected spectra present SERRS features from both dyes.

Stokes intensity than the expected for a thermal equilibrium, leading to an unusual high κ value.

When the two molecules are observed in the same spectrum, it is expected nearly the same κ for both of them if they are located at the same hot spot. A discrete dipole approximation (DDA) simulation is presented in the SI (Figure S6) to justify this assumption. The different κ values for each molecule, obtained in the same event from a distribution of hot spots on the roughened surface substrate (Figure 4c), can be explained by considering SERRS signals coming from molecules adsorbed on regions with distinct characteristic resonances. Basically, in a bianalyte experiment, when different species adsorb on the same hot spot (or in different hot spots with similar resonances), their κ values should be the same. On the other hand, when the species are adsorbed on hot spots with very different resonances, a large variation in κ in the same spectrum can be measured. Bianalyte experiments are considered the best way to prove the single-molecule capability of SER(R)S.[2,20] A limitation of the bianalyte procedure is regarding the adsorption strength of the chosen molecules, which skew the distribution of events (more spectra containing spectral signature for the molecule with higher surface affinity are observed). This limitation was circumvented by using a dye and its deuterated counterpart.[2b,21] In that case, the same chemical species, with similar adsorption behavior, was probed. The results from Figure 4, however, suggest that the single-molecule signature can also be inferred from the anti-Stokes to Stokes ratios using two different molecular species.

In order to further illustrate the single-molecule characteristics revealed by the analysis of the anti-Stokes to Stokes ratios, the κ values for each dye in a bianalyte experiment were calculated for all spectra that present nonzero signals in a 2500 spectra data set. Since κ is related to an intensity ratio, it needs to be linearized to demonstrate the Stokes- and anti-Stokes-enhanced spectra in the same scale. This was done by defining a κ' quantity according to: $\kappa' = \kappa$ for anti-Stokes-enhanced events ($\kappa > 1$), and $\kappa' = -1/\kappa$ for Stokes-enhanced events ($\kappa < 1$)

The κ' definition allows a direct comparison between their absolute value and the preferential enhancement of one of the branches (Stokes or anti-Stokes) relative to the expected from

the average SERRS distribution. For instance, $\kappa' = 2$ means that the event presents an anti-Stokes signal, relative to the Stokes, that is twice the average SERRS, and $\kappa' = -2$ represents an enhanced Stokes signal, relative to the anti-Stokes, that is twice the average SERRS.

Figure 5 shows the experimental values of κ' for both dyes obtained for all events in a data set (κ' for BG (κ'_{BG}) and CV

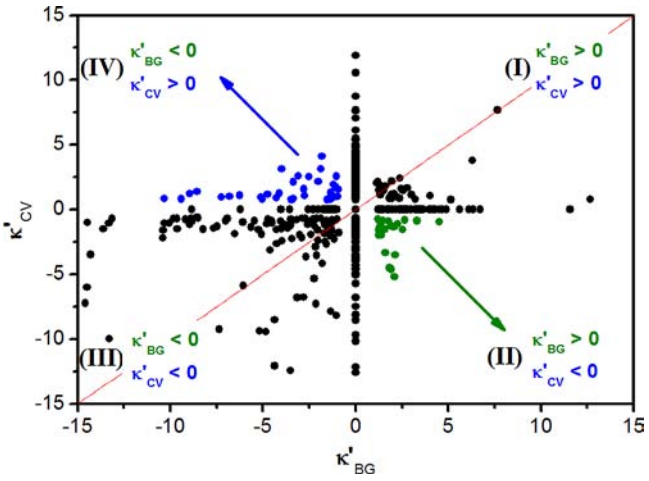

Figure 5. Experimental values of κ' for both CV and BG. Quadrant I: κ' values are positive and indicate preferential anti-Stokes enhancement for both dyes; quadrant III: κ' values are negative and indicate preferential Stokes enhancement for both dyes; quadrant II: κ' values are positive for BG and negative for CV, indicating events with preferential Stokes enhancement for CV and preferential anti-Stokes enhancement for BG; and quadrant IV: κ' values are positive for CV and negative for BG, indicating events with preferential anti-Stokes enhancement for CV and preferential Stokes enhancement for BG.

(κ'_{CV}) is reported in the x- and y-axes, respectively). The values corresponding to $\kappa'_{BG} = 0$ and $\kappa'_{CV} = 0$, along the axis in the graph, are from the events where spectral features for only one of the dyes (either CV or BG) were identified. All other κ' values in the chart are from spectra that contains contributions from both dyes, as the ones presented in Figure 4. The red line in Figure 5 is for $\kappa'_{BG} = \kappa'_{CV}$ and helps the identification of events where κ' was the same for both dyes. All points that are not intersected by the red line correspond to events where both dyes were identified and presented differential κ' values for both. All quadrants were labeled in Figure 5 to indicate the different situations.

The results of Figure 5 show that even when both dyes are observed at the same time at a given position on the electrode surface, κ' is different for each dye in the majority of the cases, which implies that the signals are originated from different hot spots. We suggest that this characteristic indicates that a small number of adsorbates ("single-molecule events") are being probed in each individual spectrum. Therefore, the analysis of Figure 5 constitutes another avenue to attest the single-molecule characteristic of SERRS that can be obtained from mixtures of dyes with different adsorption constants. Moreover, the analysis allows a better identification of events occurring at different hot spots, which is usually done by cross-correlation analysis of the peaks of each dye in a two analyte experiment. In the cross-correlation method, some degree of correlation may appear due to background emission, for instance, which can affect the interpretation.[22]

3.5. Using the Anti-Stokes to Stokes Ratios from the Bianalyte Experiments to Map the Hot Spots Resonance Profiles. The fluctuations on κ' suggest a distribution of hot spots on the surface with different resonances that enhance either the Stokes or the anti-Stokes side of the spectrum. The goal of this section is to present a model that allows the resonance envelop that contributes to the anti-Stokes to Stokes imbalance to be estimated for individual hot spots visited in each single-molecule event.

The main premise of the model is that resonance contributions at the hot spot might introduce an imbalance between the anti-Stokes and Stokes scattering cross sections; consequently, ρ (or κ) will deviate from the value measured under normal Raman (or average SERRS) conditions.

A generalized model for the plasmonic resonance involving an anti-Stokes to Stokes ratio can be represented by a squared ratio between two Lorentzian-type functions (see SI), as given by eq 2.[8b]

$$\kappa = \left(\frac{(\bar{\upsilon}_{exc} - \bar{\upsilon}_{res} - \bar{\upsilon}_{vib})^2 + \left(\frac{1}{2}\Gamma\right)^2}{(\bar{\upsilon}_{exc} - \bar{\upsilon}_{res} + \bar{\upsilon}_{vib})^2 + \left(\frac{1}{2}\Gamma\right)^2} \right)^2 \quad (2)$$

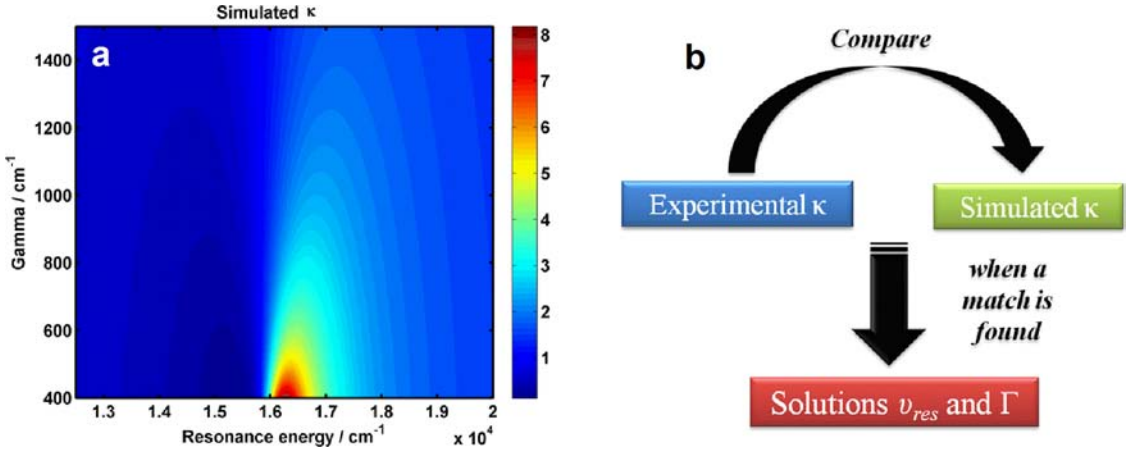

Figure 6. (a) Simulated values of κ calculated using eq 2. (b) Schematic representation of the methodology for obtaining the resonance energies in the single-molecule regime from the simulated map presented in (a).

dx.doi.org/10.1021/ja305580t | J. Am. Chem. Soc. 2012, 134, 13492−13500

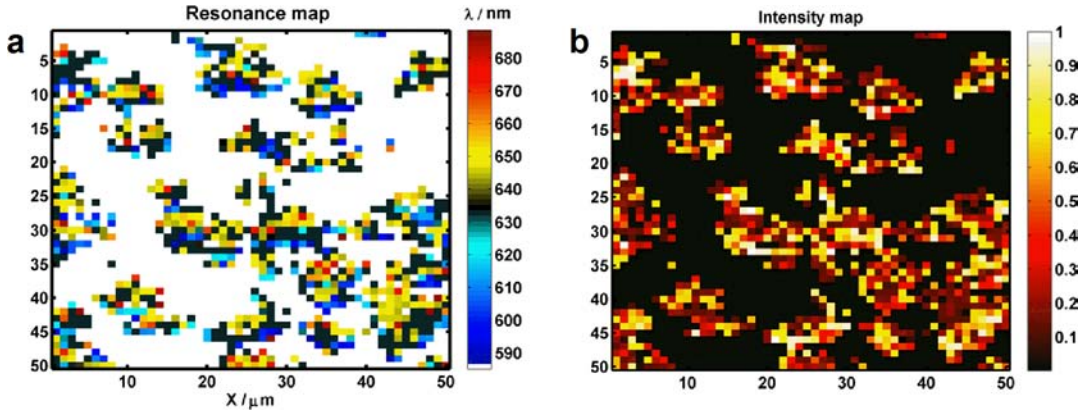

Figure 7. (a) Solutions after applying the described methodology for the resonance wavelengths shown in each point of the SERRS mapped area. (b) Experimental SERRS map of normalized intensities (anti-Stokes + Stokes) for the ∼200 cm^{-1} band in the SERRS spectra of the dyes.

where $\overline{\upsilon}_{exc}$, $\overline{\upsilon}_{res}$, $\overline{\upsilon}_{vib}$, and Γ are the laser excitation energy, the resonance frequency at the hot spot, the vibrational energy, and the width of the hot spot resonance (all in cm^{-1}), respectively. The above expression is the result of normalizing the aggregated Lorentzian (total enhancement factor) profile by the average SERRS Lorentzian profile, which was discussed in Section 3.3. Notice that the plasmonic contribution is given by the local intensities at the incident (ω) and at the scattered (ω_s) photon frequencies ($|E_{loc}(\omega)|^2|E_{loc}(\omega_s)|^2$). However, the contribution at the incident frequency does not lead to an imbalance in the anti-Stokes to Stokes ratios, and it is then removed in the calculation of κ (see SI for details). The results from Figures 3 and the model proposed in Figure S2 (SI) suggest that κ is independent of the molecular contributions, and therefore, the resonance contribution indicated in eq 2 can be attributed to the electromagnetic (LSPR) resonance at the SERRS hot spots.

A major challenge for the estimation of hot spot resonance contributions using the model suggested in eq 2 is that the width of the resonance transition (Γ) is not known *a priori*. It is possible, however, to simulate the experimental κ values for the single-molecule condition through eq 2 by using a set of different combinations of ($\overline{\upsilon}_{res}$, Γ) pairs. Figure 6a shows a 2D distribution of κ for different ($\overline{\upsilon}_{res}$, Γ) combinations for resonance values ($\overline{\upsilon}_{res}$) around the laser excitation energy (∼15 803 cm^{-1}) and a set of Γ values ranging from 400 to 1500 cm^{-1}. The solutions to the energy and width of the resonance affecting a particular experimental κ value are then obtained by searching in the simulation map the values that match to the experimental κ. When a match is found, a possible set of solutions for ($\overline{\upsilon}_{res}$, Γ) is obtained, as shown in the scheme in Figure 6b.

The resonance map of Figure 6a was set to yield simulated κ values within the same range covered by the histograms of Figure 3. The red region in the map corresponds to particular combinations of $\overline{\upsilon}_{res}$ and Γ that yield high κ values (anti-Stokes enhanced events, relative to the average SERRS). The darkest regions in the figure correspond to the combinations that yields Stokes enhanced signals. The dependence with respect to $\overline{\upsilon}_{res}$ and Γ in both branches is symmetric, i.e., narrow resonance contributions (Γ ≈ 400 cm^{-1}) close to the excitation frequency yield high enhancements to either the Stokes (dark region, $\kappa < 1$) or anti-Stokes (bright region, $\kappa > 1$) sides. This symmetry allows the following discussion to be focused on the anti-Stokes region, but the same is directly applied to the Stokes region.

Plasmonic resonances are typically broad and have some correlation to the extinction profile; however, even the sharpest resonance contribution used for the calculations in Figure 6a is not unrealistic. For instance, narrow plasmonic bandwidths (Γ ∼400 cm^{-1}) have been demonstrated for 2D arrays of interacting particles.[23] Moreover, the enhanced Raman signal should correlate with the enhancement factor profile (spectral dependence of the local field strength) which can be narrower than the extinction profile, as it can be seen in the DDA simulation presented in the SI.

Figure 6a shows that the number of possible ($\overline{\upsilon}_{res,i}$, Γ) combinations is small when the κ value is high. This allows the resonance contribution at the hot spot to be obtained through a direct comparison to the experimental κ distribution in the high κ value limit. In that case (κ values > 3), there is a narrow distribution of possible ($\overline{\upsilon}_{res}$, Γ) values such that a calculated average resonance is a good estimation of the hot spot energy. This idea is further illustrated in Figure S4 of SI. However, the number of possible combinations ($\overline{\upsilon}_{res,i}$, Γ) increases as κ approaches 1, and the assignment of the resonance energy that leads to the imbalance in anti-Stokes to Stokes ratios for such hot spots using the adopted method became ambiguous. This is because resonances centered close to the laser energy (∼15 800 cm^{-1}) as well as broad resonances far from the laser energy to the anti-Stokes side will yield values in the range $1 \leq \kappa \leq 3$.

Although it is not possible to unambiguously assign the ($\overline{\upsilon}_{res,i}$, Γ) values for those hot spots with $1 \leq \kappa \leq 3$, the resonance energy can still be estimated by using simple physical arguments. The main assumption is that the SERRS spectra from hot spots with resonance energy that matches the excitation energy will show the highest total SERRS intensities. Therefore, the hot spot resonances for κ values close to 1 is more likely to be equal (or close) to the laser energy if those events are related to large total SERRS intensities, i.e., intensities capable of single-molecule detection. In contrast, if the resonances are shifted far to the anti-Stokes or Stokes sides, small SERRS intensities from those hot spots are expected, in such a way that the observation of single-molecule spectra would not be possible. Notice that an anti-Stokes (or Stokes)-shifted resonance will generate a κ value close to 1 when Γ is large, and a broad resonance in an individual hot spot does not have a great probability of supporting single-molecule SERRS. Therefore, since all the events discussed in this section relate to single-molecule spectra, the resonances with $1 \leq \kappa \leq 3$ were assigned to coincide with the laser energy.

For the hot spots that yield $\kappa > 3$ the resonance energies, as well as their corresponding resonance widths, were then estimated by comparing the experimental κ values to the simulated ones in Figure 6a. A bin of ± 0.5 was applied to the experimental κ data to account for uncertainties into the experimental measurements and the errors due to the multiple possible $\overline{\upsilon}_{res}$ and Γ combinations. Notice that this bin size is in fact an overestimation, but it does not significantly affect the position of the hot spot resonances that generates high κ values. Using this approach, we obtained a set of plasmonic hot spot energies based on the anti-Stokes to Stokes ratios in the single-molecule SERRS regime. A spatial map of the hot spot resonances that contributed to the anti-Stokes to Stokes imbalance (in contrast to the common SERRS intensity maps) was generated, and it is presented in Figure 7a. The colors in the resonance map represent different wavelength values of the hot spot resonances (see the color bar in Figure 7a).

Figure 7a shows the estimated average resonance wavelengths for each point of nonzero intensity in the SERRS-mapped area. It is important to clarify that the area occupied by a hot spot is of a few nm^2, and it is not accessible by far-field optical methods in the visible range. Each point in the resonance map in Figure 7a corresponds to the diameter of the laser spot ($\sim 1\ \mu m^2$). Therefore, each point in the map must be interpreted as the resonance value(s) of hot spots that were visited by a given time by the molecular probes. The total SERRS intensity map is shown in Figure 7b for comparison. Each point in Figure 7b corresponds to the normalized sum of intensities for the $\sim 200\ cm^{-1}$ anti-Stokes and Stokes SERRS peaks for the dyes CV and BG. The highest intensities are represented by a yellow color, while the zero intensity events are represented by the black color.

The purpose of the normalized SERRS intensity map in Figure 7b is to illustrate the quality of the estimation of resonance energy contributions by the adopted method. In the estimated resonance map, Figure 7a, the resonances close to the laser wavelength (~ 632.8 nm) were highlighted by the black color. The previous physical argument used to estimate the energies for $\kappa \approx 1$ can be visualized by comparing the two maps. The points where the resonance was assigned to be close to the laser wavelength (black points in Figure 7a) are the ones that yielded the higher SERRS intensities (yellow points in Figure 7b), i.e., they were the hot spots that generated the highest enhancements. For the cases where the resonances start to deviate from 632.8 nm, we can identify in the SERRS intensity map smaller intensities as expected.

4. CONCLUSIONS

The model proposed here allows the fluctuations in anti-Stokes to Stokes ratios to be interpreted in terms of resonances at the plasmonic hot spots in SERS. The idea that single-molecule SE(R)RS probes molecules visiting hot spots is well established. However, the results presented here provide insights into the local resonance profile of the hot spot and reinforce the resonance characteristics of the effect. Such an interpretation for the anti-Stokes to Stokes intensity ratios permitted a model that successfully led to the estimation of the resonance energies of the enhancement factor profiles at the electromagnetic hot spots, which are of great interest in the SERS field. Moreover, the analysis permitted new interpretations in the single-molecule nature of the effect obtained in a bianalyte SE(R)RS experiment from a nonorganized substrate that contains a distribution of hot spots in the probed area.

■ ASSOCIATED CONTENT

Supporting Information

This material is available free of charge via the Internet at http://pubs.acs.org.

■ AUTHOR INFORMATION

Corresponding Author

agbrolo@uvic.ca

Notes

The authors declare no competing financial interest.

■ ACKNOWLEDGMENTS

This work was supported by the Inter-American Collaboration in Materials Research program (CIAM) from NSERC and FAPESP (FAPESP/CIAM 06/58748-5). D.P.S. acknowledges fellowships from the Department of Foreign Affairs and International Trade Canada (DFAIT) through the Emerging Leaders in the Americas (ELAP) program and from CNPq. M.L.A.T also thanks the CNPq for a research fellowship. The authors also thank Deborah R. C. Matazo and Henrique Trindade for suggestion in the usage of BG molecules for such measurements (D.R.C.M.) and for the UV−vis spectra for each dye.

■ REFERENCES

(1) (a) Kneipp, K.; Wang, Y.; Kneipp, H.; Perelman, L. T.; Itzkan, I. *Phys. Rev. Lett.* **1997**, *78*, 1667−1670. (b) Le Ru, E. C.; Etchegoin, P. G.; Meyer, M. *J. Chem. Phys.* **2006**, *125*, 204701−1−204701−13. (c) Nie, S. M.; Emory, S. R. *Science* **1997**, *275*, 1102−1106. (d) Weiss, A.; Haran, G. *J. Phys. Chem. B* **2001**, *105*, 12348−12354. (e) Liu, G. L.; Long, Y.-T.; Choi, Y.; Kang, T.; Lee, L. P. *Nat. Meth.* **2007**, *4*, 1015−1017. (f) Pieczonka, N. P. W.; Aroca, R. F. *Chem. Soc. Rev.* **2008**, *37*, 946−954. (g) Pieczonka, N. P. W.; Moula, G.; Aroca, R. F. *Langmuir* **2009**, *25*, 11261−11264.

(2) (a) Etchegoin, P. G.; Meyer, M.; Blackie, E.; Le Ru, E. C. *Anal. Chem.* **2007**, *79*, 8411−8415. (b) Dieringer, J. A.; Lettan, R. B.; Scheidt, K. A.; Van Duyne, R. P. *J. Am. Chem. Soc.* **2007**, *129*, 16249−16256.

(3) (a) Lombardi, J. R.; Birke, R. L. *J. Phys. Chem. C* **2008**, *112*, 5605−5617. (b) Lombardi, J. R.; Birke, R. L. *Acc. Chem. Res.* **2009**, *42*, 734−742. (c) Lombardi, J. R.; Birke, R. L.; Lu, T. H.; Xu, J. *J. Chem. Phys.* **1986**, *84*, 4174−4180.

(4) Fang, Y.; Seong, N.-H.; Dlott, D. D. *Science* **2008**, *321*, 388−392.

(5) (a) Shegai, T.; Vaskevich, A.; Rubinstein, I.; Haran, G. *J. Am. Chem. Soc.* **2009**, *131*, 14390−14398. (b) Park, W.-H.; Kim, Z. H. *Nano Lett.* **2010**, *10*, 4040−4048.

(6) Kneipp, K.; Wang, Y.; Kneipp, H.; Itzkan, I.; Dasari, R. R.; Feld, M. S. *Phys. Rev. Lett.* **1996**, *76*, 2444−2447.

(7) (a) Galloway, C. M.; Le Ru, E. C.; Etchegoin, P. G. *Phys. Chem. Chem. Phys.* **2009**, *11*, 7372−7380. (b) Kozich, V.; Werncke, W. *J. Phys. Chem. C* **2010**, *114*, 10484−10488. (c) Maher, R. C.; Galloway, C. M.; Le Ru, E. C.; Cohen, L. F.; Etchegoin, P. G. *Chem. Soc. Rev.* **2008**, *37*, 965−979. (d) Maher, R. C.; Etchegoin, P. G.; Le Ru, E. C.; Cohen, L. F. *J. Phys. Chem. B* **2006**, *110*, 11757−11760.

(8) (a) Haslett, T. L.; Tay, L.; Moskovits, M. *J. Chem. Phys.* **2000**, *113*, 1641−1646. (b) Brolo, A. G.; Sanderson, A. C.; Smith, A. P. *Phys. Rev. B* **2004**, *69*, 045424−1−045424−9.

(9) (a) Okamoto, H.; Nakabayashi, T.; Tasumi, M. *J. Phys. Chem. A* **1997**, *101*, 3488−3493. (b) Schomacker, K. T.; Bangcharoenpaurpong, O.; Champion, P. M. *J. Chem. Phys.* **1984**, *80*, 4701−4717.

(10) dos Santos, D. P.; Andrade, G. F. S.; Brolo, A. G.; Temperini, M. L. A. *Chem. Commun.* **2011**, *47*, 7158−7160.

(11) Wu, D.-Y.; Li, J.-F.; Ren, B.; Tian, Z.-Q. *Chem. Soc. Rev.* **2008**, *37*, 1025−1041.

(12) Markel, V. A.; Shalaev, V. M.; Zhang, P.; Huynh, W.; Tay, L.; Haslett, T. L.; Moskovits, M. *Phys. Rev. B* **1999**, *59*, 10903−10909.
(13) (a) dos Santos, D. P.; Andrade, G. F. S.; Temperini, M. L. A.; Brolo, A. G. *J. Phys. Chem. C* **2009**, *113*, 17737−17744. (b) Sant'Ana, A. C.; Alves, W. A.; Santos, R. H. A.; Ferreira, A. M. D.; Temperini, M. L. A. *Polyhedron* **2003**, *22*, 1673−1682. (c) Andrade, G. F. S.; Micke, G. A.; Tavares, M. F. M.; Temperini, M. L. A. *J. Raman Spectrosc.* **2004**, *35*, 1034−1041.
(14) Park, S. S.; Kim, K.; Kim, M. S. *Chem. Phys. Lett.* **1994**, *230*, 171−176.
(15) Galloway, C. M.; Ru, E. C. L.; Etchegoin, P. G. *Appl. Spectrosc.* **2009**, *63*, 1370−1376.
(16) Team, R. D. C. *R: A language and environment for statistical computing*; R Foundation for Statistical Computing: Vienna, Austria, 2008.
(17) (a) Goulet, P. J. G.; Aroca, R. F. *Anal. Chem.* **2007**, *79*, 2728−2734. (b) Fan, M.; Brolo, A. G. *Phys. Chem. Chem. Phys.* **2009**, *11*, 7381−7389.
(18) Jiang, J. D.; Burstein, E.; Kobayashi, H. *Phys. Rev. Lett.* **1986**, *57*, 1793−1796.
(19) Angeloni, L.; Smulevich, G.; Marzocchi, M. P. *J. Mol. Struct.* **1980**, *61*, 331−336.
(20) (a) Le Ru, E. C.; Meyer, M.; Etchegoin, P. G. *J. Phys. Chem. B* **2006**, *110*, 1944−1948. (b) Etchegoin, P. G.; Le Ru, E. C. *Phys. Chem. Chem. Phys.* **2008**, *10*, 6079−6089.
(21) Blackie, E.; Le Ru, E. C.; Meyer, M.; Timmer, M.; Burkett, B.; Northcote, P.; Etchegoin, P. G. *Phys. Chem. Chem. Phys.* **2008**, *10*, 4147−4153.
(22) Moore, A. A.; Jacobson, M. L.; Belabas, N.; Rowlen, K. L.; Jonas, D. M. *J. Am. Chem. Soc.* **2005**, *127*, 7292−7293.
(23) (a) Zhao, L. L.; Kelly, K. L.; Schatz, G. C. *J. Phys. Chem. B* **2003**, *107*, 7343−7350. (b) Zou, S. L.; Janel, N.; Schatz, G. C. *J. Chem. Phys.* **2004**, *120*, 10871−10875. (c) Zou, S. L.; Schatz, G. C. *J. Chem. Phys.* **2004**, *121*, 12606−12612.